Original Article

Combination of a human articular cartilage-derived extracellular matrix scaffold and microfracture techniques for cartilage regeneration: A proof of concept in a sheep model

Liqing Peng [a,b,1], Hao Li [a,c,1], Haoyuan Deng [a,c,1], Tianze Gao [a,c], Runmeng Li [a,c], Ziheng Xu [a,c], Qinyu Tian [a], Tianyuan Zhao [a,c], Jianwei Li [a,c], Yongkang Yang [a,c], Chao Wang [a], Shuyun Liu [a,c,**], Quanyi Guo [a,c,*]

[a] Institute of Orthopedics, the First Medical Center, Chinese PLA General Hospital, Beijing Key Lab of Regenerative Medicine in Orthopedics, Key Laboratory of Musculoskeletal Trauma & War Injuries PLA, No. 28 Fuxing Road, Haidian District, Beijing, 100853, China
[b] Department of Orthopedics, First People's Hospital of Shuangliu District, No. 120, Chengbeishang Street, Shuangliu District, Chengdu, 610200, China
[c] School of Medicine, Nankai University, No. 94 Weijin Road, Nankai District, Tianjin, 300071, China

ABSTRACT

Background: The utilization of decellularized extracellular matrix has gained considerable attention across numerous areas in regenerative research. Of particular interest is the human articular cartilage-derived extracellular matrix (hACECM), which presents as a promising facilitator for cartilage regeneration. Concurrently, the microfracture (MF) technique, a well-established marrow stimulation method, has proven efficacious in the repair of cartilage defects. However, as of the current literature review, no investigations have explored the potential of a combined application of hACECM and the microfracture technique in the repair of cartilage defects within a sheep model.

Hypothesis: The combination of hACECM scaffold and microfracture will result in improved repair of full-thickness femoral condyle articular cartilage defects compared to the use of either technique alone.

Study design: Controlled laboratory study.

Methods: Full-thickness femoral condyle articular cartilage defect (diameter, 7.0 mm; debrided down to the subchondral bone plate) were created in the weight-bearing area of the femoral medial and lateral condyles (n = 24). All of defected sheep were randomly divided into four groups: control, microfracture, hACECM scaffold, and hACECM scaffold + microfracture. After 3, 6 and 12 months, the chondral repair was assessed for standardized (semi-) quantitative macroscopic, imaging, histological, immunohistochemical, mechanics, and biochemical analyses in each group.

Result: At 3, 6 and 12 months after implantation, the gross view and pathological staining of regenerative tissues were better in the hACECM scaffold and hACECM scaffold + microfracture groups than in the microfracture and control groups; Micro-CT result showed that the parameters about the calcified layer of cartilage and subchondral bone were better in the hACECM scaffold and hACECM scaffold + microfracture groups than the others, and excessive subchondral bone proliferation in the microfracture group. The results demonstrate that human cartilage extracellular matrix scaffold alone is an efficient, safe and simple way to repair cartilage defects.

Conclusion: hACECM scaffolds combined with/without microfracture facilitate chondral defect repair.

The translational potential of this article: Preclinical large animal models represent an important adjunct and surrogate for studies on articular cartilage repair, while the sheep stifle joint reflects many key features of the human knee and are therefore optimal experimental model for future clinical application in human. In this study, we developed a human articular cartilage-derived extracellular matrix scaffold and to verify the viability of its use in

* Corresponding author. Institute of Orthopedics, the First Medical Center, Chinese PLA General Hospital, Beijing Key Lab of Regenerative Medicine in Orthopedics, Key Laboratory of Musculoskeletal Trauma & War Injuries PLA, No. 28 Fuxing Road, Haidian District, Beijing, 100853, China.
** Corresponding author. Institute of Orthopedics, the First Medical Center, Chinese PLA General Hospital, Beijing Key Lab of Regenerative Medicine in Orthopedics, Key Laboratory of Musculoskeletal Trauma & War Injuries PLA, No. 28 Fuxing Road, Haidian District, Beijing, 100853, China.
E-mail addresses: clear_ann@163.com (S. Liu), doctorguo_301@163.com (Q. Guo).
[1] These authors contributed equally to this work.

sheep animal models. Clinical studies are warranted to further quantify the effects of hACECM scaffolds in similar settings.

1. Introduction

Articular cartilage is characterized by its limited intrinsic healing capacity [1]. As a result, cartilage injuries often extend beyond the articular surface, encroaching upon the subchondral bone. If left unaddressed, these osteochondral defects may further degenerate into osteoarthritis (OA), thereby inducing a variety of clinical symptoms [2,3]. Hence, the successful amelioration of focal cartilage defects is paramount to prevent the onset of osteoarthritis. Several treatment modalities for cartilage injuries currently exist, spanning from conservative non-invasive approaches to minimally invasive surgical procedures [4]. However, no treatment to date has proven capable of fully restoring the damaged tissue to the level of healthy, native cartilage [5]. In fact, microfracture (MF) stands as the primary treatment due to its affordability and simplicity. Yet, this reparative strategy remains suboptimal. The resulting tissue comprises fibrocartilage, which demonstrates inferior performance compared to native articular hyaline cartilage in withstanding shear and compressive forces [6,7]. Thus, there is an urgent clinical need for the development of a single-step, readily accessible, and cost-effective cartilage repair therapy. Ideally, this approach should minimize the duration of surgery and consistently produce hyaline-like cartilage repair. One plausible strategy could involve augmenting microfracture surgery with scaffold use. This consideration is not only based on the cost-effectiveness of the procedure but also on the widespread accessibility of microfracture and its potential for comparable outcomes to cell-based procedures [8–10].

Recently, tissue engineering strategies have emerged as a promising avenue for joint tissue regeneration [11]. Components extracted from the extracellular matrix (ECM) are increasingly being recognized as valuable resources for bioengineering due to their proven ability to induce desirable cell-specific responses [12]. Notably, cartilage ECM scaffolds are primarily composed of type II collagen, which has been empirically demonstrated to foster chondrogenic differentiation even in the absence of growth factors [13]. Further, numerous studies have documented that seeding human macrophages onto such scaffolds results in the upregulated expression of interleukin-8 (IL-8) and basic fibroblast growth factor (bFGF), both of which are known to be chondro-inductive [14–16]. These findings collectively underscore the potential of human articular cartilage-derived extracellular matrix (hACECM) as a promising scaffold material for cartilage repair in tissue engineering. In recent years, our research team has concentrated on the treatment of articular cartilage injuries using scaffolds derived from natural articular cartilage extracellular matrices. These scaffolds have been fashioned from cartilage sections sourced from human cadaveric joints, leveraging decellularization techniques. The resulting scaffolds, in combination with autologous chondrocytes and encased within fibrin glue, have been utilized to address cartilage defects, producing promising clinical outcomes [17]. Additionally, these ECMs, prepared via this method, have been incorporated with a variety of bioactive substances, yielding noteworthy therapeutic effects across diverse animal models [18,19].

Nevertheless, these studies do bear inherent limitations. Firstly, the clinical investigations assessed outcomes solely through follow-up examinations and non-invasive techniques, omitting histological evaluations of the repaired cartilage tissue. Secondly, the majority of related basic research involves small animal models, which may not directly translate to clinical applications. Thus, two significant queries persist: Can the human articular cartilage extracellular matrix (hACECM) solely enhance full-thickness cartilage repair? Can the fusion of hACECM with the microfracture (MF) technique augment the outcome of microfracture cartilage repair? We propose that comprehensive large animal experiments are imperative for addressing these questions. To our understanding, no randomized controlled trials comparing hACECM and MF in large animal models have been conducted to date. Therefore, we established a standalone hACECM scaffold implantation group to verify the reparative efficacy of this scaffold when directly implanted into animals without the need for in vitro autologous cell culture loading. The primary goal of this study is to formulate a reliable and effective large animal experimental model, and to histologically compare the therapeutic impacts of hACECM and MF within a sheep cartilage defect model. Our hypothesis postulates that the repair of full-thickness femoral condyle articular cartilage defects is enhanced when the hACECM scaffold is implanted in conjunction with microfracture, compared to the defect left untreated.

2. Materials and methods

2.1. Production of hACECM scaffold

The process of ECM scaffold preparation has been previously described [20]. Briefly, articular cartilage was pulverized and decellularized by gradient centrifugation to produce an ECM homogenate. This was then injected into cylindrical molds of 7 mm diameter and subjected to a freezing gradient from $-20\ °C$ to $-80\ °C$, followed by a 24-h freeze-drying process. Porous, oriented scaffolds were fabricated through a dehydration process and treatment with water-soluble carbodiimide.

2.2. Characterization of hACECM scaffold

2.2.1. Scanning Electron Microscopy and mechanical testing
The hACECM scaffold was lyophilized for 24 h, fixed on an aluminum stage, and sputter coated with gold prior to observation. The microstructure was examined using a Scanning Electron Microscope (SEM) (S-4800 field emission scanning electron microscope; Hitachi).

The biomechanical characteristics of the scaffolds were analyzed using a microcomputer-controlled electronic universal testing machine in a compression test. Scaffolds of dimensions $5 \times 5 \times 1.2$ mm were prepared, pre-compressed by 5%, with a compression rate of 4.5 mm/min and a precompression load of 0.8 N. Following 20 cycles, a formal test was performed with a maximum compression of 10%. Four samples from each group were tested and a representative strain–stress curve was presented.

2.2.2. Histological staining
hACECM scaffolds were fixed in 4% para-formaldehyde for 48 h, embedded in paraffin, and sectioned into slices of 7 μm thickness. Hematoxylin and eosin (HE) staining identified cellular components, while Trypan Blue (TB) and Safranine O (SO) staining assessed the presence of the cartilaginous matrix. The fibrous collagen structure was assessed through Sirius Red staining procedures.

2.2.3. Human chondrocytes isolation and cultivation
Human chondrocytes were isolated from human knee joint cartilage from amputee patients, sliced into $1 \times 1 \times 1$ mm pieces, and digested using 0.2% type II collagenase (Sigma–Aldrich) for 2 h in Dulbecco's Modified Eagle Medium (DMEM). The cell suspension was then centrifuged at 1500 rpm for 5 min and cultured in DMEM with 10% fetal bovine serum (Sigma–Aldrich). Once 90% confluence was reached, the third passage of cells was used to determine scaffold cytocompatibility.

2.2.4. Cell viability staining and Scanning Electron Microscopy
Cell viability within the scaffold was assessed using a live/dead assay

kit (Beyotime). Briefly, human chondrocytes were cultured in DMEM/F12 (10% FBS) medium at a concentration of 5×10^5 cells per 20 μL for 3 days. The cell-loaded scaffolds were washed with sterile PBS three times, incubated in a PBS solution containing 0.05% (v/v) calcein-AM and 0.2% (v/v) propidium iodide at 37 °C for 30 min, and then rinsed with sterile PBS. The samples were visualized using a fluorescence confocal microscope (Leica TCS-SP8; Leica Microsystems) and analyzed using Imaris software (Bitplane).

For Scanning Electron Microscopy (SEM), the cell-loaded scaffolds were obtained 3 days after seeding with human chondrocytes. The scaffolds were fixed in 2.5% (v/v) glutaraldehyde for 2 h at room temperature, dehydrated in graded ethanol concentrations, and subjected to critical point drying (EM CPD300; Leica). After 30 min of sputter coating with gold, the cell-loaded scaffolds were observed using SEM.".

2.3. Cytocompatibility studies of hACECM scaffold

2.3.1. Cell proliferation assays

The proliferative response of cells within the hACECM scaffold extracts was quantitatively assessed on days 1, 3, and 7 utilizing the CCK-8 kit (Dojindo Laboratory, Japan). Both the scaffold extracts and the cells were added to 96-well tissue culture polystyrene (TCPS) plates. At each time point, a CCK-8 working solution (reagent: medium = 1:10) was introduced to each well and incubated at 37 °C for 2 h. Wells without hACECM scaffold extract served as controls. The absorbance of the test solution (n = 4 per group) was measured at 450 nm using a microplate reader (Beckman, Fullerton, CA).

To visualize cell proliferation via EdU staining, the Cell-Light EdU in vitro kit (RiboBio, Guangzhou, China) was used. Human chondrocytes were cultured on cell slides within a 24-well plate at an approximate density of 1×10^4 cells per well for 24 h. Subsequently, they were treated with DMEM/F12 containing 1% FBS and hACECM scaffold extracts for an additional 24 h. The medium was then substituted with a 50 mM EdU solution, followed by a period of incubation. The standard procedures were utilized for staining with EdU and DNA using DAPI. Each EdU staining group consisted of three replicates.

2.3.2. Cell migration assay

The recruitment capacity of the hACECM scaffold was evaluated using a Transwell system (Corning, USA) with pure DMEM/F12 medium serving as a negative control. Briefly, 100 μL of serum-free DMEM/F12 containing 2×10^4 resuspended human chondrocytes were positioned in the upper chamber, while 600 μL of serum-free DMEM/F12 and hACECM scaffold were placed in the lower chambers. After a 12-h and 24-h incubation at 37 °C, cells were fixed with 4% paraformaldehyde for 20 min and stained with crystal violet. Three replicates per group were performed. The number of cells that migrated through the membrane was quantified using ImageJ software.

2.3.3. Accelerating effect of hACECM on chondrogenic differentiation of human chondrocytes

Chondrogenic differentiation characteristics of the scaffold were verified by implanting human chondrocytes into the hACECM scaffold. The sterilized hACECM scaffold was placed on a 24-well plate and human chondrocytes were seeded onto the scaffold and cultured with chondroblast induction medium (CIM, Cyagen Biosciences, China). After 3 days, scaffolds were collected and qualitative analysis of chondrocyte differentiation was performed using HE, TB, SO, and COLII immunohistochemical staining. For immunohistochemical staining, sections were deparaffinized, rinsed in PBS three times, and subjected to antigen retrieval in a microwave. Samples were washed in PBS, treated with 0.5% (v/v) hydrogen peroxide for 10 min, and incubated with primary antibodies against collagen type II (COL 2A1) (Abcam) overnight at 4 °C. Following incubation with secondary antibodies (ABC Kit; Vector Laboratories Inc), sections were developed using diaminobenzidine (Vector Laboratories) and counterstained with hematoxylin.

Quantitative real-time reverse transcriptase polymerase chain reaction (qRT-PCR) experiments were conducted to analyze cartilage-related gene expression. In brief, scaffolds were collected, and total RNA was extracted using commercial TRIzol reagent (Invitrogen, USA). Reverse transcription to cDNA was carried out using a ReverTra Ace qPCR RT Kit. A Step-One Real-Time PCR system (Applied Biosystems) with SYBR Green PCR Master Mix (Genestar, USA) was used for the real-time PCR procedure. To obtain credible results, melt curves were assessed following the amplification procedure, and nonspecific amplification was checked. The gene expression was evaluated relative to the housekeeping gene by the ΔCt method. Four independent assays were performed for each value.

2.4. Implantation of hACECM scaffold in sheep for efficacy study

2.4.1. Study Design

Twenty-four sheep were randomly allocated into four groups of six each: the scaffold and microfracture group (hACECM/MF Group), the scaffold-only group (hACECM Group), the microfracture group (MF Group), and the blank control group (Control Group). The detailed methodology about time point for chondral defect surgery and evaluation (Table 1) was as follows: Firstly, two of six sheep were received left hind leg surgery at the surgery day (0 month), and then received right hind leg surgery 3 months later. And at the 6 months time point, these sheep were euthanized for evaluation. Secondly, another two of six sheep were received left hind leg surgery at the surgery day (0 month), and then received right hind leg surgery 6 months later. And at the 12 months time point, these sheep were euthanized for evaluation. Lastly, two of six sheep were received left hind leg surgery at the surgery day (0 month), and then received right hind leg surgery 9 months later. And at the 12 months time point, these sheep were euthanized for evaluation. According to the experimental design, cartilage defects were created in the weight-bearing areas of the femoral medial and lateral condyles of both knee joints, with three observation points set at 3, 6, and 12 months. Each time point encompassed eight defects per group. Upon sampling, MRI scans of the knee joint were performed after preserving the knee capsule. The capsule was then opened for gross visual examination and photographed. Micro-CT scans of the femoral condyle were carried out, followed by histological examinations after the decalcified repaired area and tissue block were sectioned. This comprehensive evaluation compared the effect of cartilage tissue repair in each group.

2.4.2. Surgical procedure

All procedures were reviewed and approved by the Institutional Animal Care and Use Committee at the Chinese PLA General Hospital. The surgical procedure was modified according to previous studies [21–24]. In detail, preoperatively, the sheep were weighed, and atropine sulfate (0.3 mg) was administered intramuscularly 30 min in advance.

Table 1

Time point for chondral defect surgery and evaluation of each group.

Number	Time point for chondral defect surgery and evaluation				
	0 month	3 months	6 months	9 months	12 months
1	Left hind leg	Right hind leg	Euthanized for evaluation		
2	Left hind leg	Right hind leg	Euthanized for evaluation		
3	Left hind leg		Right hind leg		Euthanized for evaluation
4	Left hind leg		Right hind leg		Euthanized for evaluation
5	Left hind leg			Right hind leg	Euthanized for evaluation
6	Left hind leg			Right hind leg	Euthanized for evaluation

Anesthesia was also administered intramuscularly at a dosage of 0.2 mg/kg of xylazine hydrochloride. Sheep were then secured in the lateral position on the operating table, routinely disinfected, and the distal lower extremity was wrapped with a disposable sheet.

A surgical incision approximately 7 cm long was made along the anterior aspect of the sheep's knee, slightly medial and 0.5 cm from the upper edge of the patella down to the tibial tuberosity. The subcutaneous fascia was separated layer by layer to expose the quadriceps and patellar ligament. The muscle was incised in the direction of the medial femoral quadriceps muscle for approximately 4 cm, with the incision extending downwards to the tibial tuberosity. To expose part of the femoral condyle, the knee joint was straightened, dislocating the patella laterally, and then flexed. The medial condyle was fully exposed by removing part of the fat pad and synovial tissue in the operative area and retracting the tissue to both sides. The lateral condyle was exposed by stripping the synovial membrane along the anterior rectus knee ligament and pulling the hook to the lateral side to retract the anterior rectus knee ligament. Relatively flat areas on the medial and lateral condyles were selected for weight-bearing, and full-thickness articular cartilage defects in the lateral and medial femoral condyles were made using a 7-mm-diameter corneal trephine under sterile conditions, while preserving the subchondral bone. After moderate trimming of the defect perimeter, treatments were carried out according to the group assignments (Fig. 1).

In the Control Group, no treatment was conducted after cleaning the defect with iodophor saline. For the MF Group, several holes were drilled vertically into the subchondral bone using a 1.0 g needle to a depth of about 1 cm, until a yellowish and bloody fluid exuded from the holes. After coagulation, the cavity was rinsed with saline. In the hACECM Group, a pre-prepared hACECM scaffold was placed after absorbing the fluid in the defect area with sterile gauze. The hACECM/MF Group underwent a similar process as the MF Group, followed by placement of the hACECM scaffold. After ensuring the scaffold was stable and intact, the wound cavity was irrigated with saline, and the patella repositioned and the joint capsule, tendons, muscles, fascia, and skin sutured layer by layer.

Postoperatively, sheep were ear-tagged according to their groups. Following recovery from anesthesia, the sheep were allowed to stand and limp on their own, kept in a warm and dry environment without immobilization of the operated limbs, and were allowed to move freely and gradually become fully weight-bearing. The wound was disinfected with iodophor daily for 7 days.

2.4.3. Macroscopic observations

Animals were euthanized by intramuscular injection of an anesthetic overdose at predetermined postoperative intervals of 3, 6, and 12 months. The lower limb was dissected from the mid-femur, ensuring the preservation of knee joint-associated soft tissues. Subsequent to the MRI of the knee joint, we opened the joint capsule for gross examination, Micro-CT scanning, and specimen processing for histological examination and scoring.

Post-MRI of bilateral knee joints, the knee capsule was opened, revealing the femoral condyle defect area for direct observation. We assessed the following parameters: (1) presence of inflammatory tissue surrounding the surgical incision, (2) clarity of joint fluid, noting the presence of any turbid, flocculent substances or inflammatory secretions, (3) signs of inflammatory adhesions, synovial membrane and fibrous connective tissue proliferation, synovial hypertrophy in the joint cavity, (4) the degree of cartilage growth in the repaired area, new cartilage filling volume, and integration with adjacent tissues, (5) the surface morphology of healthy cartilage, and the presence of cartilage wear, tear, and bone flap formation in other regions. Upon completion of observations, the surrounding soft tissues were removed, each knee joint ligament attachment point was separated, and the intact femoral condyle was preserved, photographed, and scored. We blindly scored cartilage repair tissues, referencing the macroscopic scoring system suggested by the International Cartilage Repair Society (ICRS) [25].

2.4.4. Biochemical analysis

Following the opening of the knee joint, we punched out the repair region using a corneal trephine of the same size as that used for creating the cartilage defects. Collagen content per sample was determined by crushing the samples and applying a DMMB colorimetric kit (Nanjing jiancheng Inc., China).
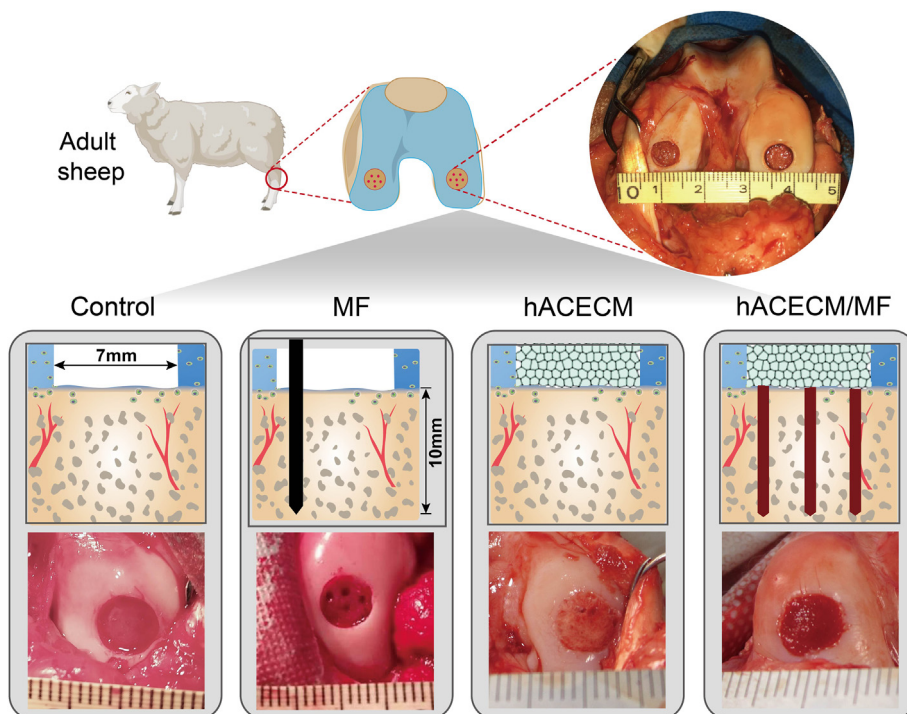

Fig. 1. The process of operation and schematic diagram of each group.

2.4.5. Biomechanical test

Furthermore, we evaluated the biomechanical properties of the cartilage by measuring Young's modulus in three samples per group using the In Situ Nanomechanical Test System (Hysitron, USA). The radius of curvature of the conspherical diamond probe tip was 100 mm. The trapezoidal load function was used on each indent site with loading (10 s), holding (5 s), and unloading (10 s). The cylindrical loading device was perpendicular to the RA and moved forward by 2000 nm at 200 nm/s.

2.4.6. MRI acquisition and assessment

Six and twelve-month postoperative animals were euthanized, and bilateral lower limbs were disconnected, preserving the intact joint capsule and knee-associated soft tissues. We conducted scans using a 7.0 T animal MRI instrument (Bruker BioSpin, Germany) with adjusted T2W1 lipid suppression sequence. Post-scan, sagittal cross-sectional images of the repaired area were selected and saved for the evaluation of the repair effect in each group and the regenerative morphology of the repaired cartilage defect area. The degree of joint degeneration was assessed according to the WORMS scoring system, including cartilage signal and morphology, subarticular bone marrow abnormality, and bone attrition [26]. Higher scores represent more severe joint degeneration. Three blinded observers performed the scoring.

2.4.7. Micro–computed tomography

Femoral condyles were scanned and reconstructed using Micro-CT after completing gross visual observation scoring. We conducted further quantification analysis on the rectangular ROI containing the original osteochondral defect, including measurements of bone mineral density (BMD), bone volume/total volume (BV/TV), trabecular thickness (Tb.Th), and trabecular separation (Tb.Sp) of the repaired area.

2.4.8. Histological and immunohistochemical staining

Upon the completion of the prior experiments, the femoral condyles from the sheep were sectioned using a table saw, ensuring the preservation of at least 3 mm of peripheral tissue and 1 cm of subchondral bone beneath the repaired area. These specimens were fixed in 4% paraformaldehyde for 72 h. A decalcifying solution of 10% EDTA was prepared, replacing the solution every two days. Once the tissue was fully decalcified, it underwent a dehydration process and was subsequently embedded in paraffin. Utilizing an automatic slicer, sections were generated at a thickness of 5 μm. These sections were extended onto slides with a spreader, followed by a baking period of 2–3 h at 60 °C. Sections were then dewaxed using a gradient of xylene and ethanol, from absolute ethanol to 80%. Following these processes, tissue sections were stained with Hematoxylin & Eosin, Safranin O/Fast green, Toluidine blue, and Sirius red. Three blinded observers utilized the macroscopic scoring system proposed by Goebel et al. [27] to complete the histological scoring.

Further, an immunohistochemical assay was performed for COL2 detection using a COL2 antibody (1:100, II-II6B3, DSHB), as previously described. Briefly, sections were incubated overnight at 4 °C with primary antibodies against COL2, followed by incubation with goat anti-mouse IgG (1:200; Cat# NB7539; Novus) for 1 h at room temperature. The reaction was visualized by application of a DAB substrate kit.

2.5. Statistical analysis

Statistical data analysis was conducted using the Student's t-test for two groups with parametric data, and one-way analysis of variance (ANOVA) followed by Tukey's post hoc test for multiple groups with parametric data. Two-way variance (ANOVA) with Tukey's post hoc test was utilized for comparisons between different genotypes and procedures. Non-homogeneous variance data was analyzed using the rank-sum test. All statistical evaluations were conducted using SPSS statistical software (version 25.0, Chicago, IL, USA) or GraphPad Prism 8 (Graph-Pad Software Inc., San Diego, CA, USA). All data are reported as the mean $\pm$ SD of the mean. Significance was defined as values of $p < .05$.

3. Results

3.1. Characterization of the hACECM scaffold

Fig. 2A illustrates both the macroscopic viewpoint and the intricate microstructure of the human acellular cartilage extracellular matrix (hACECM) scaffold as observed under Scanning Electron Microscopy (SEM). Notably, the SEM image confirmed an interconnective, three-dimensional porous architecture inherent in the scaffold. A stress-–strain curve, representative of the hACECM scaffold's mechanical properties, is depicted in Fig. 2B.

To ascertain the effectiveness of the decellularization process employed for hACECM, we carried out Hematoxylin & Eosin (HE) staining alongside specific tissue staining techniques. Fig. 2C delineates the HE staining outcome, which successfully demonstrated an absence of nuclear remnants post-decellularization. Additionally, Toluidine Blue (TB), Safranin O (SO), and Sirius Red (SR) staining techniques corroborated the preservation of cartilage matrix even after decellularization.

The viability of human chondrocytes in the hACECM scaffold was examined by executing live/dead cell staining post 3 days of culture. Predominantly, cells within the hACECM scaffold manifested green fluorescence (indicative of living cells) with a minute proportion exhibiting red staining (indicating dead cells), as portrayed in Fig. 2D. Subsequently, using SEM, we observed the attachment and migration of human chondrocytes within the interconnecting pores of the hACECM scaffold over the 3-day culture period (Fig. 2E).

### 3.2. Biological functions of the hACECM scaffold

Quantitative analysis using Cell Counting Kit-8 (CCK-8) was employed to assess the hACECM scaffold's role in stimulating human chondrocyte proliferation (Fig. 3A). Based on the results derived from 5-ethynyl-2′-deoxyuridine (EdU) fluorescence staining (Fig. 3B–C), we established that human chondrocyte showed significant proliferation at 24 h within both the hACECM scaffold extracts group and the control group. However, the hACECM scaffold notably amplified human chondrocyte proliferation in comparison with the control group.

The hACECM scaffold's impact on human chondrocyte migration was evaluated via a Transwell migration assay (Fig. 3D). Crystal violet staining revealed a considerable enhancement in human chondrocyte migration within the hACECM scaffold group relative to the control group after both 12 and 24-h intervals. Further quantitative analysis reinforced that the hACECM scaffold substantially augmented human chondrocyte migration compared to the control group (Fig. 3E).

Post 3 days of hACECM scaffold culture, changes in the expression of chondroblast-related genes were detected by RT-PCR. The expression levels of COL2, COL1, ANCN, and SOX9 were assessed (Fig. 3G). At day 3, the expressions of COL2, ANCN, and SOX9 in the hACECM scaffold group were not significantly higher than those in the control group. Interestingly, COL1 expression in the hACECM scaffold group was lower than that in the control group, although the difference was not statistically significant.

3.3. Macroscopic view and ICRS macroscopic scoring

The knee joints of the experimental animals exhibited adequate flexion and extension mobility, with no discernible joint ankylosis or flexion contracture. Upon dissection post-sampling, the joint fluid from the joint capsule was clear and devoid of turbidity. Evident in some of the control and microfracture (MF) groups at the 6-month mark were severe cartilage degeneration, medial condyle collapse, exposure of subchondral bone, and the development of bone redundancy at the medial condyle edge. All group specimens exhibited healthy incision healing in the sheep knee with no visible signs of inflammatory nodules or liquefied necrosis
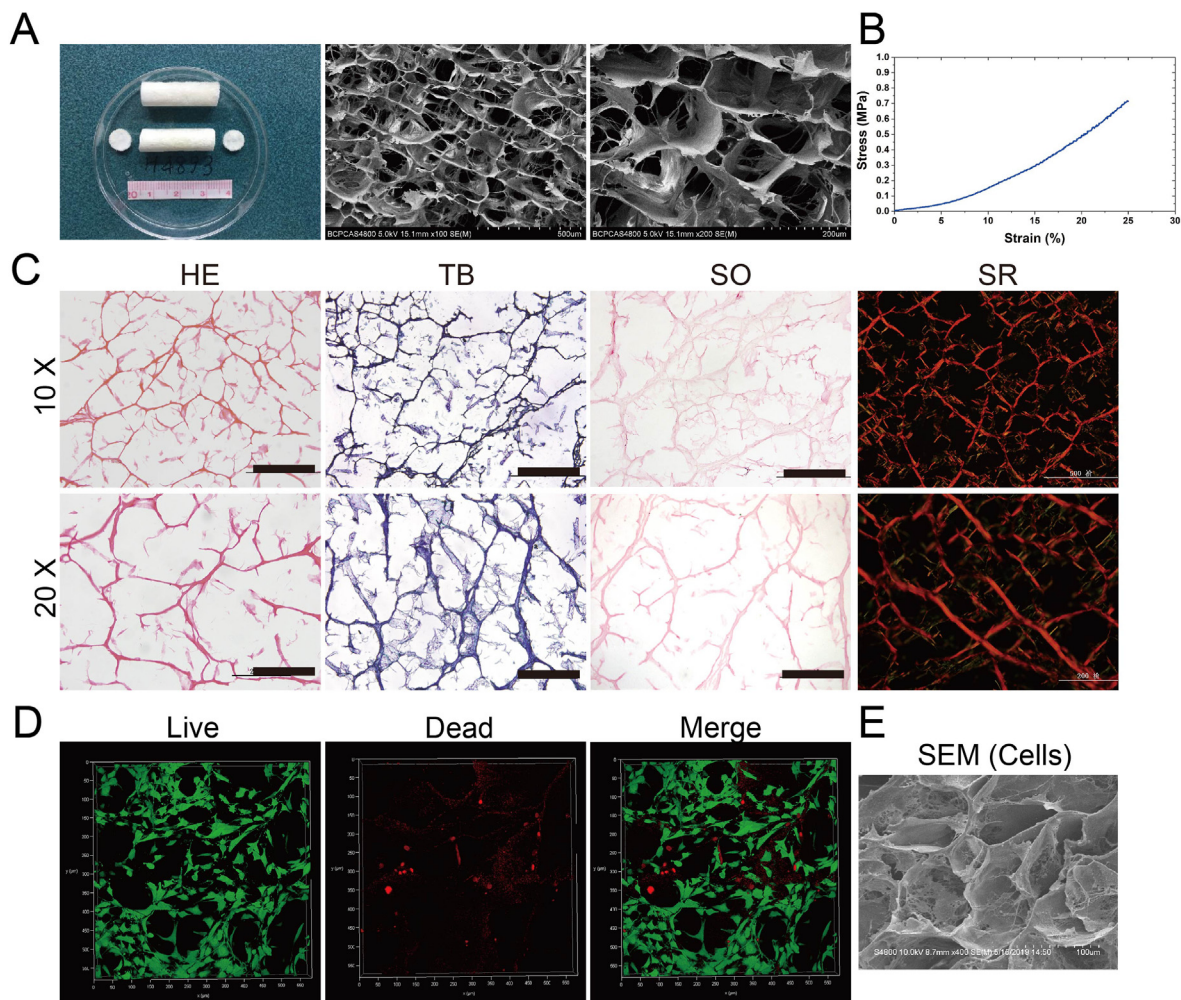
Fig. 2. The physicochemical, histological, and biocompatible properties of hACECM scaffolds. (A) Macroscopic view and SEM of the hACECM scaffold. (B) Stress–strain curve of the hACECM scaffold. (C) The representative slides of hematoxylin&eosin (HE), trypan blue staining (TB), safranine O (SO) and sirius red (SR) staining for the hACECM scaffold. (10x field of view. Scale bar = 200 μm, 20x field of view. Scale bar = 200 μm) (D) Live/dead cell analysis for the hACECM scaffold on which human chondrocytes were seeded for 3days, with representative images showing live (green) cells, dead (red) cells. (E) Scanning electron micrographs of the hACECM scaffold on which human chondrocytes were seeded for 3 days.

(Fig. 4A).

A detailed macroscopic description for each group is as follows.

(i) Control group: At the 3-month mark, an absence of surface tissue was visible in the defect area, which also demonstrated substantial collapse and subchondral bone resorption. In the 6-month group, the defect filling showed marginal improvement over the 3-month group but underfilled cartilage layers remained. The 12-month group revealed a significant fibrous tissue filling in most defect areas with reduced collapse and resorption in comparison to the previous groups.

(ii) MF group: By 3-months, part of the defect area was filled with new tissue. In the 6-month group, the filling area and height increased compared to the 3-month group. At 12-months, the defect area was predominantly filled, the surface of the new tissue remained rough, and there was a mild collapse boundary between the defect area and the surrounding area.

(iii) hACECM group: At 3-months, the defect filling was less than in the MF group. In the 6-month group, the filling area increased significantly compared to the 3-month group. By 12-months, new tissues completely filled the defect areas, appearing smoother and color-matched to surrounding tissues.

(iv) hACECM/MF group: At 3-months, the defect area filling was more substantial than in the other three groups. The 6-month group showed more filled areas than the 3-month group. At 12-months, new tissues completely filled the defect areas, matching the height of surrounding tissues.

The results were obtained after blinded scoring of each group at each time point according to the ICRS gross body view scoring system (Fig. 4B, Table 2): at the 3-month time point there was no statistical difference between the groups. At the 6-month time point, the mean score was highest in the hACECM group, similar in the MF and hACECM/MF groups, and similar in the hACECM and hACECM/MF groups at the 12-month time point, compared to the MF group were higher. Statistics showed no statistical difference in the scores of MF, hACECM, and hACECM/MF in the 6-month group and 12-month group results showed higher and statistically different scores than the Control group.

3.4. Biochemical and biomechanical results

The total collagen content was evaluated using a dimethylmethylene blue (DMMB) colorimetric kit, as represented in Fig. 4C. The data revealed that the hACECM/MF group generated an increased amount of collagen in the repaired tissue compared to the Control, MF, and
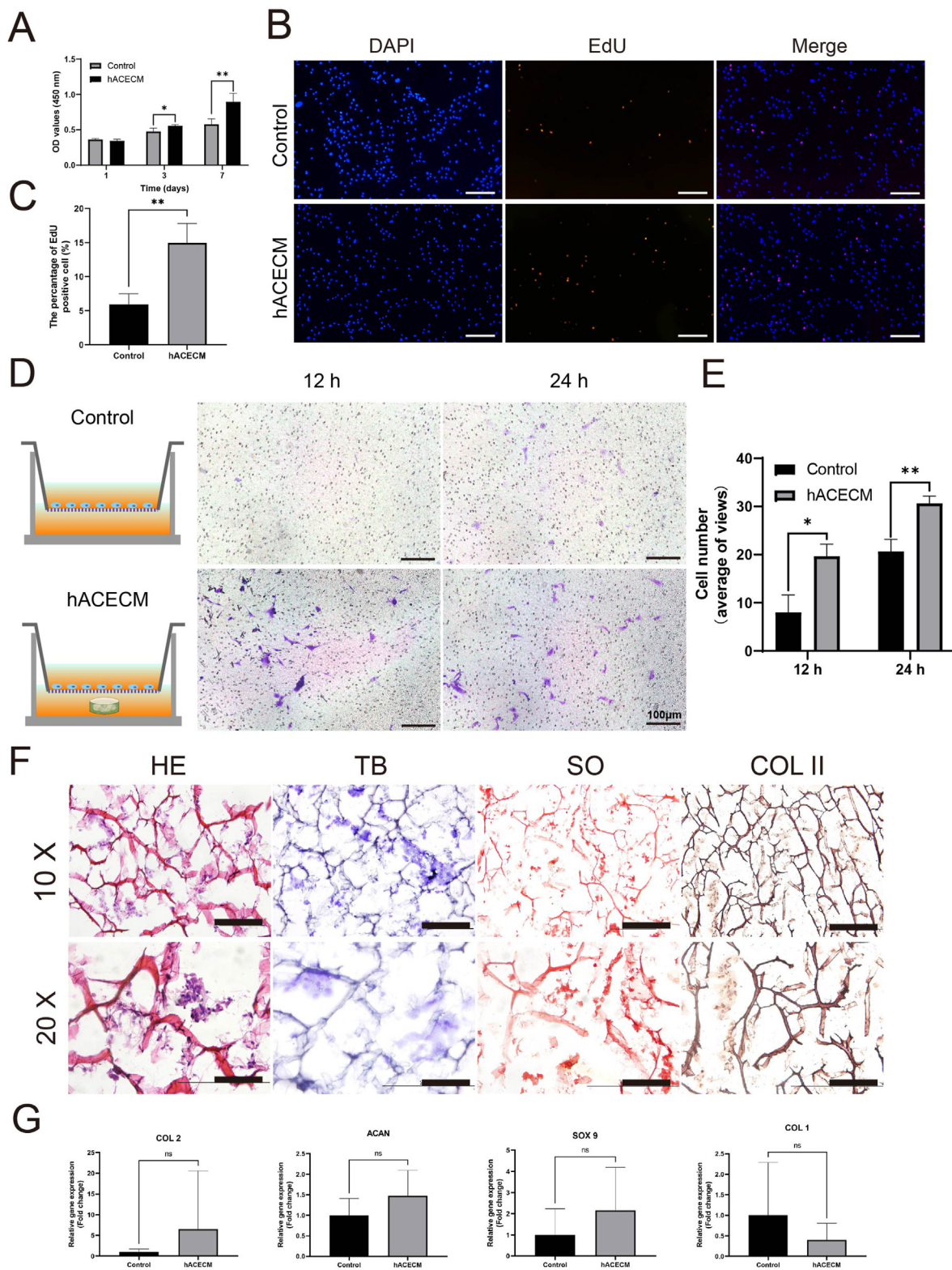
Fig. 3. The biological properties of hACECM scaffolds. (A) Quantification of OD values in CCK-8 experiments of human chondrocytes after treating with the hACECM scaffold extract for 1,3,7 days. (B,C) EdU staining and fluorescence quantification of human chondrocytes after treating with the hACECM scaffold extract for 24 h. Scale bar = 100 μm. (D) Schematic of cell chemotaxis assay in a Transwell system, and crystal violet staining of migrated human chondrocytes after seeding for 12 and 24 h. Scale bar = 100 μm. (E) Statistical analysis of migrated human chondrocytes. (F) The representative slides of HE, TB, SO and collagen type 2 immunohistochemical staining for the hACECM scaffold after human chondrocytes seeded for 3days. Scale bar = 200 μm. (G) Cartilage-related gene expression of human chondrocytes on the hACECM scaffold for 3 days: collagen 2 (COL 2), Aggrecan (ACAN), SRY-Box Transcription Factor 9 (SOX9), and collagen 1 (COL 1) (Data are expressed as mean ± SD. *P < .05; **P < .01; ***P < .001; ****P < .0001; ns not statistically significant.).

hACECM groups at both the 3-month and 6-month intervals. These findings coherently corroborate our preceding results.

The mechanical properties of the repaired tissue were further evaluated by analyzing the compression modulus (Fig. 4D). The findings suggested that tissues repaired at the 12-month mark generally demonstrated a superior compression modulus relative to those repaired at the 6-month point across all experimental groups. However, no statistical significance was found within each group at either time point. Intriguingly, the modulus of the repaired tissue in the Control group tended to be higher compared to the MF, hACECM, and hACECM/MF groups at both examined intervals.

3.5. MRI evaluation and WORMS results

The evaluation proceeded with a 7.0 T small animal magnetic resonance imaging (MRI) scan conducted on the sheep knee joints at the 6-month and 12-month intervals to visualize the cartilage signal, subchondral bone signal, and the signal from the surrounding femoral condyles in the area of repair (Fig. 4E).

MRI results in the Control group in 6-month showed no obvious tissue filling in the area of the cartilage defect, and the surrounding cartilage signal was disorganized and interrupted in the area of the defect. The subchondral bone in the area of the defect and its deep surface near 1 cm were partially accompanied by disorganized abnormal signals, indicating that there was no obvious repair of the cartilage and its subchondral bone tissue in the area of the defect or even destruction towards the deep surface of the defect in this group. the cartilage signal was interrupted in the area of the cartilage defect in the 6-month MF group, and most of the filling tissue in the area showed bone tissue signals, some of which were disorganized and abnormal, and the signal in the subchondral bone had a small number of abnormal signals and was generally normal. This indicates that there may be an overgrowth of subchondral bone occupying the area of the cartilage defect. In 6-month group, the area of the cartilage defect in the hACECM group showed the same signal as the surrounding cartilage tissue, with a thickness comparable to that of the surrounding tissue, but the normal signal in the junction area with the surrounding cartilage was interrupted and filled with a disorganized abnormal signal. There was a mild abnormality in the subchondral bone signal. This indicates that most of the defect area in this group may have been repaired, but the surrounding area was poorly integrated with normal tissue. 6-month hACECM/MF group showed a smaller area of cartilage defect than before, and a small portion of it showed the same signal as the surrounding normal cartilage tissue, and the central area showed a disorganized abnormal signal. No abnormalities were seen in the subchondral bone.

MRI findings in the 12-month Control group showed that the area of defective cartilage was partially filled with tissue with a different signal from the surrounding cartilage, with a round-like cystic abnormal signal area in the subchondral bone below the defective area. The MRI of the 12-month MF group showed that the cartilage signal was interrupted in the area of the cartilage defect, and most of the filled tissue in the area showed bone tissue signal, and the bone tissue signal was higher than that of the 6-month group, and no obvious cartilage signal was seen on the surface. In the hACECM group, the cartilage defect area was completely filled, and the cartilage signal was basically present within it. The surface of the repair area was smooth, and the thickness of the cartilage signal was significantly increased and similar to the surrounding cartilage than in the 6-month group, and the perimeter of the repair area was fused with the border. The MRI results of the 12-month hACECM/MF group showed that the cartilage defect area was fuller than that of the 6-month group, the defect was completely filled, the surface of the repaired area was smooth, the thickness of the repaired area was similar to that of the surrounding cartilage, and it was fused with the surrounding border. Some of the subchondral bone was slightly higher than the surrounding planes and clearly defined abnormal signals were seen.

Regarding the WORMS scores for the knees (Fig. 4F), the total scores revealed that the best neo-tissue quality and repair was observed in the knees from the hACECM group (6 months: 10.25 ± 1.30; 12 months: 8.25 ± 1.48) and hACECM/MF group (6 months: 10.75 ± 2.38; 12 months: 9.25 ± 1.09), especially at 12 months, followed by the MF group (6 months: 15 ± 0.71; 12 months: 14 ± 1.22). The Control group (6 months: 22.5 ± 3.04; 12 months: 20.75 ± 3.27) had higher WORMS scores than the MF group, which had the worst results, in which no obvious repair or regeneration was observed.

The cartilage signal and morphology scores were better in the hACECM and hACECM/MF groups than in the other two groups (Fig. 4G). Regarding subchondral bone attrition (Fig. 4H), the damage to subchondral bone in the MF group was obvious, followed by the Control group, but all three groups exhibited an inflammatory response. During the retired restoration period, the subchondral bone of the hACECM and hACECM/MF groups were the most complete, and the marrow abnormality (Fig. 4I) and inflammation scores were also present a lower tendency among all groups.

3.6. Micro-CT analysis

CT scans and reconstructions were performed using animal Micro-CT on the intercepted femoral condyles of the 3-month, 6-month, and 12-month groups of sheep (Fig. 5), and bone parameters related to the cartilage repair area were evaluated after analysis of BMD, BV/TV, Tb.Th, and Tb.Sp data.

The results at the 3-month time point: all groups showed destruction of subchondral bone integrity in the defect area and showed bone tissue collapse and resorption. the subchondral bone collapse in the defect area in the Control group was larger, with a diameter comparable to the defect area and a depth of about 1 cm, and sparse and less dense bone tissue was visible at the bottom of the collapse. the subchondral bone density in the defect area in the MF group was reduced, and there was a cystic cavity under the bone plate with a clear boundary and a diameter comparable to the defect area. The diameter of the cavity was comparable to the extent of the defect. In the hACECM group, the diameter of subchondral bone collapse in the defect area was comparable to the extent of the defect, and the depth of collapse was less than that in the first two groups, and the base of the collapsed area and the surrounding area were filled with loose, low-density bone with unclear boundary boundaries, showing a tendency to grow above the defect. The border of the defect was surrounded by high-density dense bone tissue, which was filled with loose low-density bone, with more filled bone tissue than the hACECM group.

The results at the 6-month time point: the Control group still had large subchondral bone defect with partial filling of surrounding bone, subchondral bone continuity was not restored, there was still a large cavity defect surrounded by slightly lower bone density. The MF group had complete filling of subchondral bone in the defect area, new bone tissue fused with the surrounding. In the hACECM group, the bone in the defect area was basically filled and fused with the surrounding bone, and the joint surface was not smooth. In the hACECM/MF group, the defect area was basically filled with bone and fused with the surrounding bone. The deep subchondral bone surface was slightly poorly formed with a cavity-like defect, the bone density in the filled area was similar to the surrounding area, and the bone density around the cavity was slightly higher, and the bone trabeculae were more closely arranged.

The results at the 12-month time point: there was still a small amount of bone defect in the center of the defect area in the Control group, the continuity of the subchondral bone plate was not completely restored, and the subchondral bone surface was rough. In the MF group, the defect area was completely filled with subchondral bone, and the new bone tissue was fused with the surrounding area. Some of it was still above the plane of the surrounding normal subchondral bone plate, the extent of bone proliferation was roughly the same as the defect area, and its deep bone was loudly arranged similarly to the surrounding normal area. the bone in the defect area of the hACECM group was completely filled and
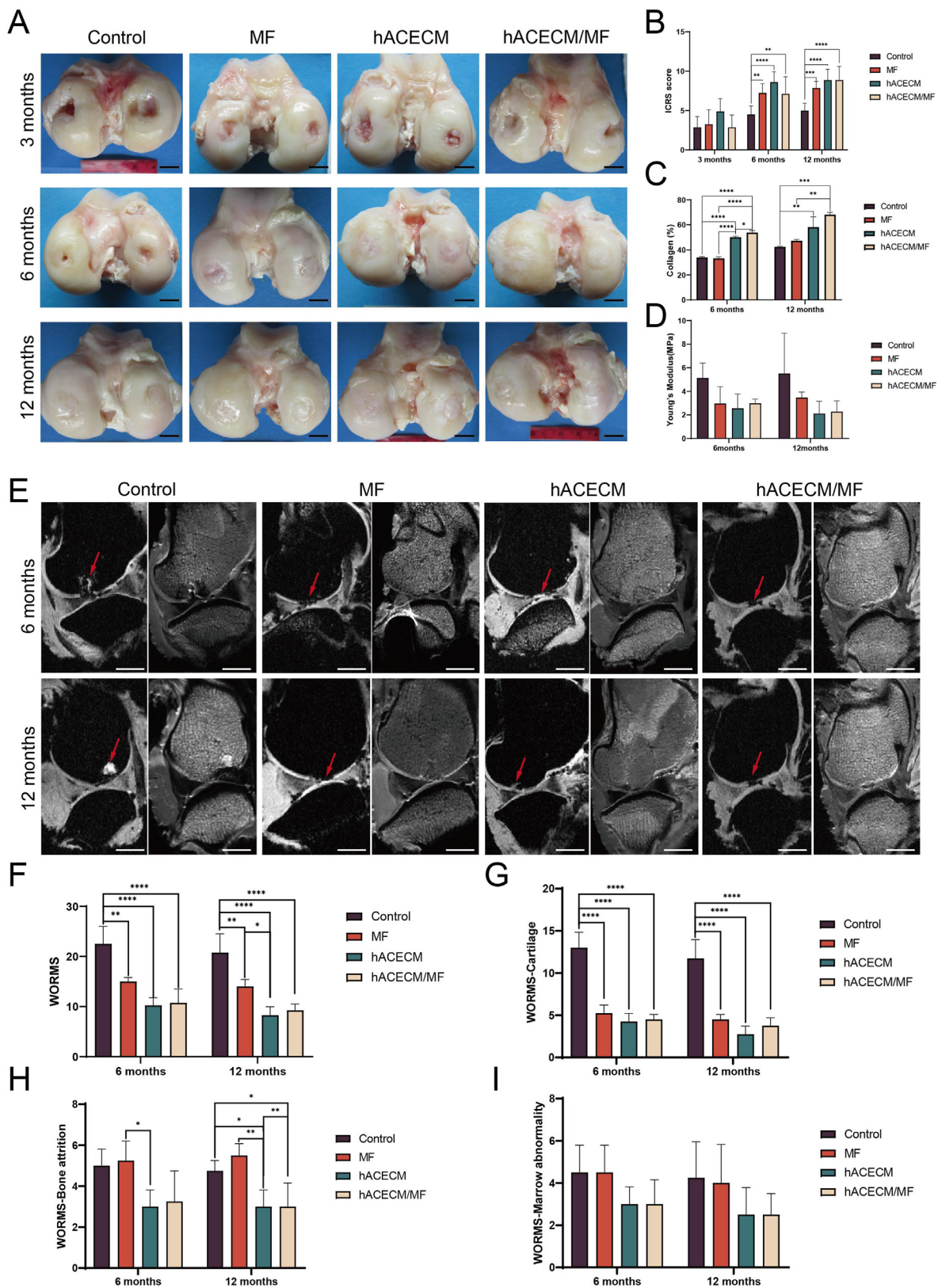
Fig. 4. Macroscopic and MRI evaluation of the repaired tissues. (A) Representative macroscopic images of the repaired tissues at 3, 6 and 12 months postsurgery. Scale bar = 1 cm. ICRS scores (B), Collagen content (C) and Young's modulus (D) in the repair areas of each group at 6 and 12 months postsurgery. (E) T2W1 images of different sheep knees at 6 and 12 months postsurgery. Scale bar = 1 cm. WORMS evaluation (F), WORMS cartilage (G), WORMS bone attrition (H) and WORMS marrow abnormalities (I) of MRI images (Data are expressed as mean ± SD. *P < .05; **P < .01; ***P < .001; ****P < .0001; ns not statistically significant.).

Table 2
ICRS scores evaluated on each group.

Group	Time point		
	3 months	6 months	12 months
Control	2.875 ± 1.356	4.500 ± 1.069	5.000 ± 0.926
MF	3.325 ± 1.832	7.250 ± 1.165	7.875 ± 0.835
hACECM	4.375 ± 1.847	7.625 ± 3.068	8.875 ± 1.356
hACECM/MF	2.875 ± 1.553	7.125 ± 2.167	8.875 ± 1.727

fused with the surrounding bone. The articular surface was flatter and basically in the same plane as the surrounding normal area. In the hACECM/MF group, the defect area was filled with bone and fused with the surrounding area, and some of the defect areas had a small amount of bone defect in the center. The bone density of the deep subchondral bone filling area was slightly lower than the surrounding normal area, and the trabeculae were more densely arranged than the surrounding normal area.

Analysis of bone correlation parameters after scanning reconstruction of specimens from each group of time points (Fig. 5B–F).

BMD: At the 3-month time point, the BMD results showed that the MF, hACECM, and hACECM/MF groups were significantly higher than the Control group (P < .05), while there was no significant CT difference between these three groups; at the 6-month time point, the results were the same as before, with the highest mean value in the hACECM/MF group; at the 12-month time point, the BMD of the MF and hACECM/MF groups was significantly higher than that of the Control group (P < .05), while the hACECM and the Control groups were not significantly different, and the Control groups were not significantly different, with the MF group having the highest mean value.

BV/TV: The MF, hACECM, and hACECM/MF groups were significantly higher than the Control group at the 3-month time point (P < .05); the results at the 6-month time point were the same as before, with the hACECM/MF group having the highest mean value among the four groups and the MF and hACECM groups having similar mean values. at the 12-month time point, there was no significant difference among the four groups, and the data showed that the MF and hACECM/MF groups had relatively higher mean values.

Tb.Th: The MF group had the highest relative value at the 3-month time point, the hACECM and hACECM/MF groups had similar values, and the Control group had the lowest value, and the results showed no significant difference between the groups; the Control group had the highest relative value at the 6-month time point, the MF and hACECM/MF groups had similar values, and the hACECM group had the lowest value, and the results showed no significant difference between the groups; the MF group had the highest relative value at the 12-month time point, the hACECM/MF group had a higher value than the hACECM group, and the Control group had the lowest value, and the results showed no significant difference between these groups.

Tb.Sp: the results at the 3-month time point showed that the Control group was significantly higher than the three groups MF, hACECM and hACECM/MF (P < .05), while there was no significant difference between these three groups; the results at the 6-month time point were the same as before, the Control group was significantly higher than the remaining three groups (P < .05), and there was no significant difference between the lower three groups; there was no significant difference between the groups at the 12-month time point, but the values showed that the mean of the Control group was still highest, and the remaining three groups had similar values.
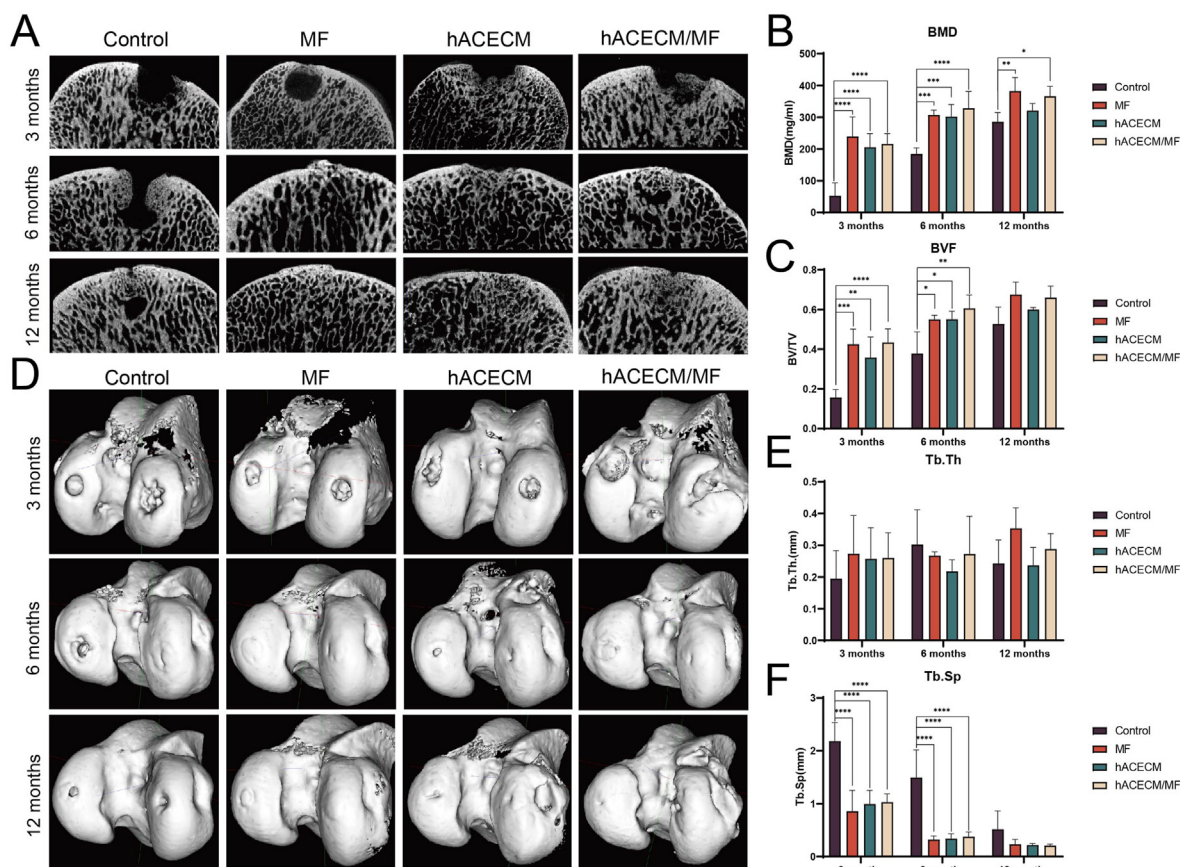
Fig. 5. CT evaluation of the repaired tissues. (A) Sagittal CT images of different sheep knees at 3, 6 and 12 months postsurgery. Quantitative analysis of (B) BMD and (C) BV/TV in the defect area. (D) 3D reconstructed CT images of different sheep knees at 3, 6 and 12 months postsurgery. Quantitative analysis of (E)Tb.Th and (F) Tb.Sp of each group (Data are expressed as mean ± SD. *P < .05; **P < .01; ***P < .001; ****P < .0001; ns not statistically significant.).

3.7. Histological and immunohistochemical analyses

HE staining: the repair area was not filled to fullness in all groups at the 3-month time point (Fig. 6). the Control group had a significant defect in the repair area, which was deep to the subchondral bone, with disorganized fibrous tissue agglomerates and some cartilage tissue deep into the subchondral bone. the MF group had a better filling of the defect area than the Control group, with a mild depression on the surface and interrupted cartilage continuity, with fibrous tissue in the center of the defect area and disorganized subchondral bone morphology, forming a capsule-like structure surrounded by dense fibrous tissue. In the hACECM group, the defect area was mostly filled with fibrous tissue, no clear cartilage formation was observed, the surface of the new tissue was rough and divided, the structure was disorganized, and the subchondral bone was depressed downward. The defective area of Control group was still obvious, filled with fibrous tissue, the deeper area of subchondral bone was damaged, with obvious boundary with the surrounding normal tissue and poor fusion. the surface of the defective area of MF group was complete, the new tissue was slightly higher than the surrounding normal tissue plane, the thickness of new cartilage was thinner than normal cartilage, the surface was rough, the arrangement of subchondral bone was disordered, and part of the new tissue cartilage was deep into the subchondral bone area. the ECM group repair area was basically repaired, the surface was flatter and smoother, the cartilage thickness was thinner than the normal area, some oval chondrocytes were visible in the surface tissue, the arrangement was not regular, and the border was fused with the surrounding normal tissue. In the hACECM/MF group, the defective area was basically repaired, the cartilage surface was flatter, the cartilage thickness in the repaired area was more consistent, slightly thinner than normal cartilage, and some oval chondrocytes were visible in the area. Part of the border was divided from normal cartilage tissue, and part of the cartilage tissue at the interface grew into the subchondral bone. The subchondral bone in the repaired area was intact and aligned smoothly. the cartilage in the repaired area in the Control group at the 12-month time point grew poorly, with no obvious boundary and depressed tissue in the central area. The cellular arrangement of the new tissue was disorganized, the surface was not flat, and some of the superficial fractures were visible. The subchondral bone arrangement was disordered, with localized agglomerated fibers. the repaired tissue in the MF group basically filled the defect area, and the surface was mildly depressed at the border. the surface of the new tissue was uneven, and the cells within it were mostly spindle-shaped, with localized agglomerated clusters. The subchondral bone plate was intact, and the subchondral bone plate in contact with the cartilage surface was uneven. in the hACECM group, the repair tissue filled the defect area, and the surface was slightly uneven. the new cartilage tissue was mostly oval chondrocytes with a disorganized arrangement, and the formation of tidal lines between the cartilage layer and the calcified layer was obvious. In the hACECM/MF group, the repair tissue completely filled the defect area, and the surface was flat. The new cartilage tissue was mostly composed of oval chondrocytes, which were arranged longitudinally and parallel to the articular surface. The subchondral bone was intact and flat, with good union.

The hACECM group had red staining of normal cartilage tissue around the defect and no matrix red staining on the surface of the repaired area at the 3-month time point. In the hACECM group, the normal cartilage tissue around the repair area was red stained, and the new tissue in the repair area had no obvious matrix red staining, and the deep tissue solid green staining was weaker than the normal subchondral bone around the repair area. In the hACECM/MF group, the cartilage in the repair area was partially red-stained, the coloring was more uniform, the coloring was similar to that of the surrounding normal cartilage, the coloring at the junction was slightly lighter, and the coloring in the cartilage and subchondral bone areas was clearly demarcated. The cartilage in the repair area of the MF group had no red staining or lighter and uneven staining in most areas, and the red stained parts were mostly clumped,

with uneven staining at the same level. the cartilage in the repair area of the hACECM group was red stained, with more uniform staining, and similar staining to the surrounding normal cartilage, with slightly lighter staining in the upper 1/3 of the cartilage area, and obvious staining demarcation between the cartilage and subchondral bone areas. In the hACECM/MF group, the cartilage in the repair area was red-stained, with a more uniform coloring, similar to the surrounding normal cartilage coloring, and a slightly lighter coloring in the middle 1/3 of the cartilage area, with a clear demarcation between the cartilage and the subchondral bone area coloring.

Sirius red staining: The repair area of each group at the 3-month time point appeared red or yellow under polarized light, with strong double refractive properties and tightly arranged type I collagen; the repair area of the Control group at the 6-month time point was partially non-refractive, with some surface areas of strongly yellow refractive type I collagen; the repair area of the MF group was red or yellow tightly arranged type I collagen with a few weakly refractive green type III collagen fibers. In the ECM group, the surface and deep areas were mostly yellow or red type I collagen, with a sparse reticulation of multicolored type II collagen and some fine fibrillar weakly refractive type III collagen. In the MF group, the surface and deep areas of the repaired area were mostly red dense strongly refractive type I collagen, and the fibers in the repaired area were arranged in a disorganized manner. In the hACECM/MF group, the surface of the repaired area was flat, and the repaired area was filled with multi-colored, loose reticular and weakly refractive type II collagen and green, fine-fibrillated type II collagen.

Based on the above staining results, analysis of the results using the macroscopic scoring system (Fig. 7) showed that the 3-month time point, all groups had more significant defects and no good cartilage tissue filling in the cartilage region, so all scores were lower (Control group: 14.67 $\pm$ 0.47, MF group: 17.33 $\pm$ 1.89, hACECM group. 17.67 $\pm$ 0.47, hACECM/MF group 18.000 $\pm$ 0.82), and there was no statistical difference between the groups. The results at the 6-month time point showed that the scores of the MF group (25.667 $\pm$ 0.94), hACECM group (30.33 $\pm$ 1.25), and hACECM/MF group (34.33 $\pm$ 2.87) were significantly higher than those of the Control group (16.00 $\pm$ 0.82) and were statistically different, and both the hACECM and hACECM/MF groups had significantly higher scores than the MF group. The 12-month time point results were consistent with the 6-month results, with the MF group (28.33 $\pm$ 0.94), the hACECM group (33.67 $\pm$ 1.25), and the hACECM/MF group (37.33 $\pm$ 2.887) all having significantly higher scores than the Control group (20.000 $\pm$ 2.36) and were statistically different, and the scores in both the hACECM and hACECM/MF groups were significantly higher than those in the MF group.

3.8. Collagen orientation and distribution in the repaired cartilage

We performed Sirius red staining of the femoral condyles in each group at 3, 6, and 12 months postoperatively, observed the collagen in the regenerated area of the defect under a polarized light microscope, and applied the imageJ plug-in to analyze the collagen orientation and distribution in each layer of the repaired area according to published protocol [28](Fig. 8A). The collagen in the superficial region of normal cartilage tended to be horizontally oriented, and the collagen in the deep region tended to be vertically oriented. We found that at 3 months postoperatively the cartilage layers in the defective area were discontinuous in each group, with no significant collagen repair tissue filling. At 6 months postoperatively, all three groups except the control group had tissue filling, but the thickness and collagen orientation characteristics of the repaired area were different among the groups. As shown in Fig. 8B and C, in the superficial repair area the collagen entanglement orientation in the control and MF groups was dispersed between 0 and 60°, while the two groups applying hACECM were concentrated between 0 and 10°; in the deeper area, the collagen orientation in the control, MF and hACECM groups was widely dispersed, and the collagen orientation in the hACECM/MF group was similar to normal cartilage close to
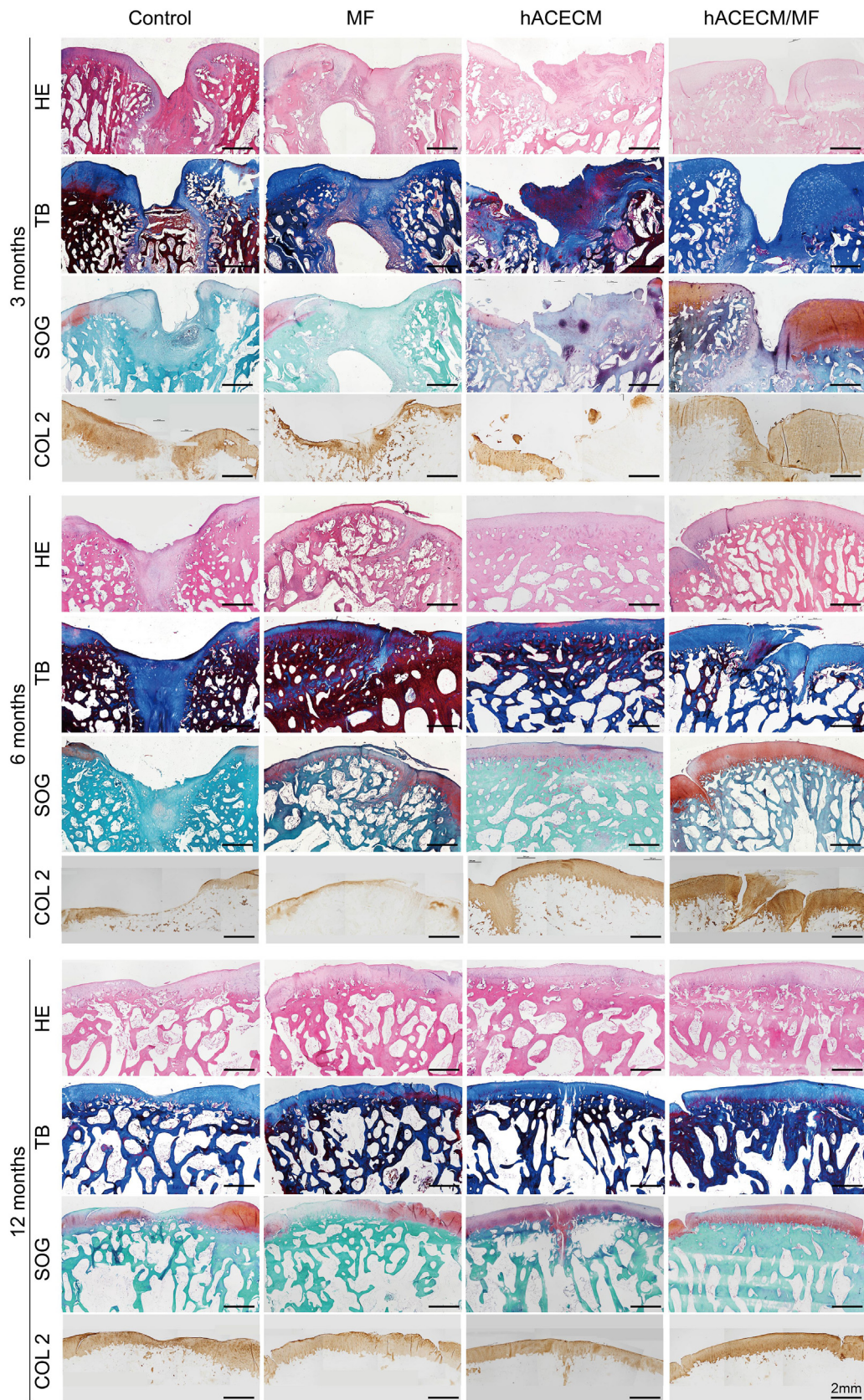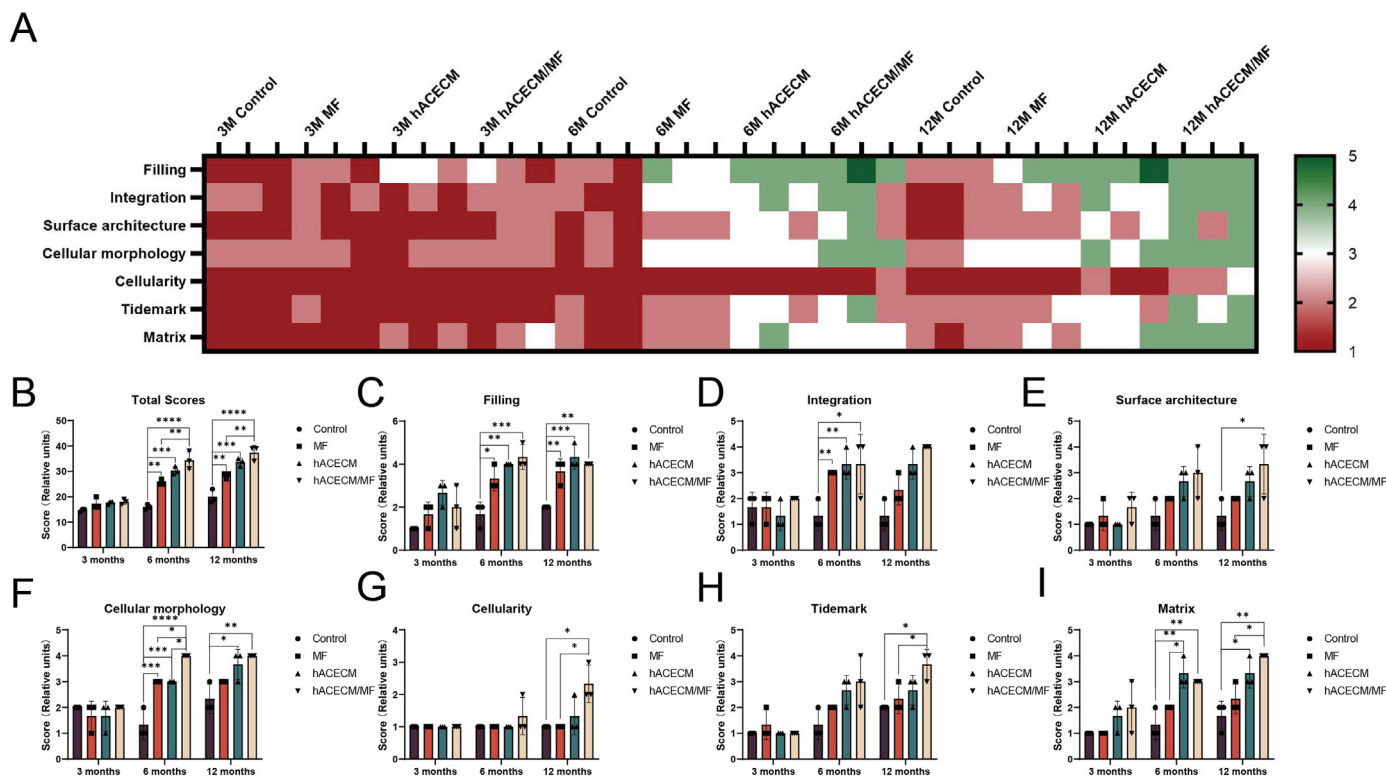
Fig. 6. The representative slides of HE, TB, Safranine O&Fast Green (SOG) and collagen type 2 immunohistochemical staining for the repaired tissues.

Fig. 7. (A) The macroscopic scoring system heat map of each group at 3, 6 and 12 months postsurgery. Total scores (B), filling (C), integration (D), surface architecture (E), cellular morphology (F), cellularity (G), tidemark (H), matrix (I) based on modified O'Driscoll scores of the repaired tissues (Data are expressed as mean ± SD. *P < .05; **P < .01; ***P < .001; ****P < .0001; ns not statistically significant.).

vertical. In the superficial repair area, the two groups with hACECM were still concentrated between 0 and 10°, and the collagen orientation of the MF group was also shifted to the horizontal direction compared with that at 6 months, but the collagen of the control group was still chaotically distributed; in the deep area, the collagen of the control and MF groups was dispersed between 30 and 70°. In the deeper region, collagen dispersion was between 30 and 70° in the control and MF groups, and the hACECM/MF group maintained a structure similar to that of natural cartilage. Therefore, the hACECM/MF group was better able to regenerate and reconstruct an orthogonal collagen network similar to natural cartilage compared to the other groups, both at 6 months and 12 months postoperatively.

4. Discussion

In this investigation, we initially fabricated a hACECM scaffold utilizing a physicochemical decellularization technique, examined its physicochemical properties and biocompatibility, and subsequently assessed its potential for repairing full-thickness chondral defects with and without the MF technique in a sheep model. Our findings indicated that both toluidine blue and safranin O staining tests were positive following the decellularization procedure. This study further demonstrates that the hACECM scaffold possesses a natural 3D porous microstructure, excellent cytocompatibility, and commendable compressive strength. Furthermore, in vitro cytocompatibility assays revealed the hACECM scaffold's capacity to facilitate the proliferation, migration, and phenotype preservation of human chondrocytes. Although the underlying mechanisms remain undetermined, the hACECM scaffold appeared to aid in chondral repair and cartilage regeneration in vivo.

Articular cartilage defects, due to their limited self-healing capacity, necessitate innovative surgical repair strategies. The microfracture technique, first introduced two decades ago and currently the most widely used method for cartilage repair due to its relative simplicity and

minimization of patient trauma [29], was also employed as a therapeutic modality in this experiment. This surgical strategy aims to mobilize pluripotent stem cells from the bone marrow cavity to the site of repair, thereby producing loose granulation tissue and upregulating the expression of fibrogenesis-related proteins [18,30]. However, microfracture does exhibit limitations in cartilage repair. While it manages to fill and repair the defect in the early stages, the newly formed tissue primarily consists of fibrocartilage, incapable of fulfilling the weight-bearing and frictional demands of joint hyaline cartilage, thus leading to suboptimal long-term prognosis [7]. Therefore, there remains a pressing clinical need to develop a simple, cost-effective approach to augment the microfracture technique in cartilage repair.

Recently, extracellular matrix (ECM) derived scaffolds have piqued researchers' interest due to their capacity to provide both structural and functional signals to cells [31,32]. Furthermore, in contrast to other biomaterials sourced from type I collagen, ECM from articular cartilage is naturally rich in type II collagen and has been demonstrated to foster robust chondrogenesis in vitro and in vivo [28,33]. Articular cartilage-derived ECM inherently contains an array of bioactive factors, including collagens, proteoglycans, ECM glycoproteins, ECM-regulatory proteins, ECM-affiliated proteins, and secreted factors, all of which are presumed to possess inherent chondro-inductive properties [34]. Consequently, in the present study, we utilized hACECM as a biological scaffold for the repair of articular cartilage defects. The biocompatibility of the fabricated scaffold with human chondrocytes was confirmed by Live/Dead staining and SEM results. To verify the biological functions of the hACECM scaffold, we conducted a series of in vitro studies. Notably, the CCK-8 and EdU experiment results revealed that the hACECM scaffold significantly enhanced cell proliferation. Additionally, the hACECM scaffold stimulated human chondrocyte migration in vitro, indicating that this biomaterial holds promise for endogenous cartilage regeneration. To confirm the chondro-inductive effects of hACECM, we performed quantitative real-time reverse transcriptase polymerase chain reaction
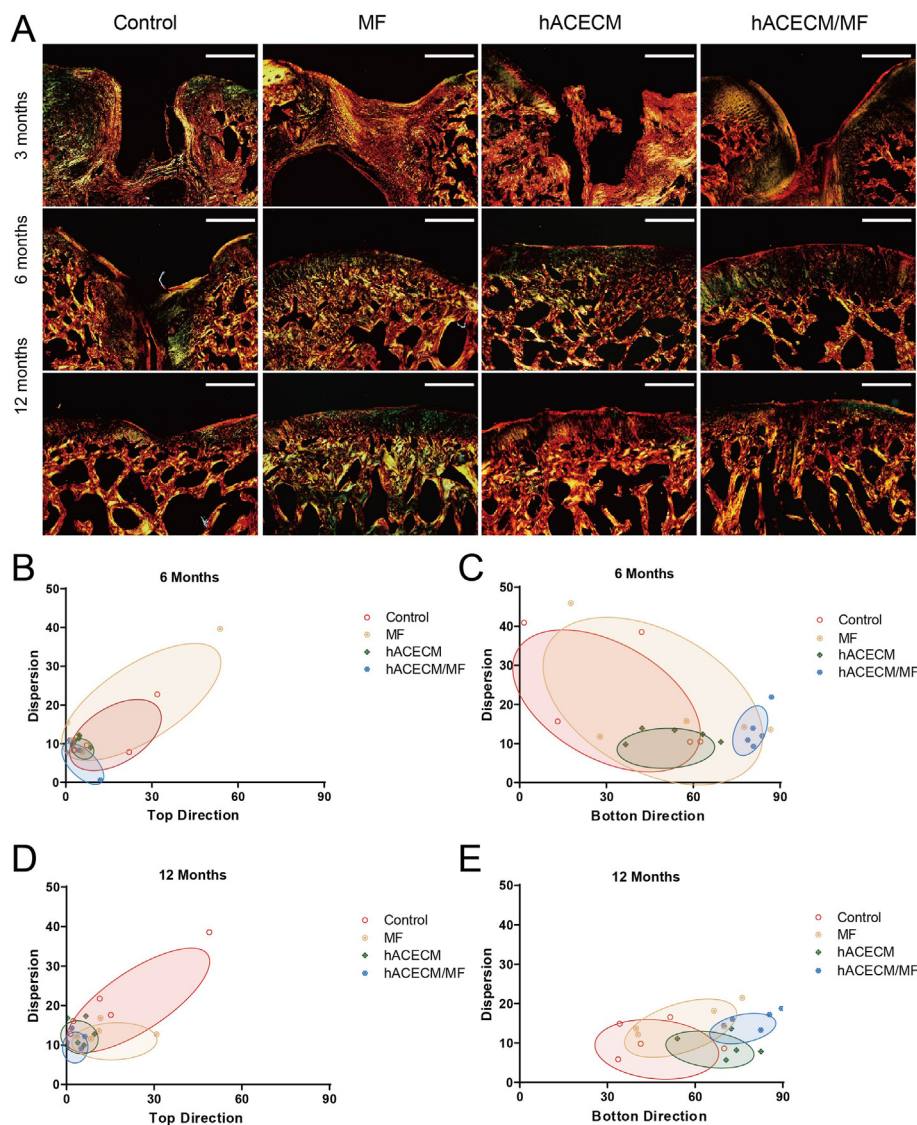
Fig. 8. Quantitative analysis of the collagen fiber orientation in the repaired tissues within the repaired tissue. (A)The representative slides of Sirius red (SR) staining for the repaired tissues. (B, C) Evaluation of the collagen fiber orientation in the superficial zone and deep cartilage zone within the repaired tissues at 6 months. (D, E) Evaluation of the collagen fiber orientation in the superficial zone and deep cartilage zone within the repaired tissues at 12 months (Data are expressed as mean ± SD. *P < .05; **P < .01; ***P < .001; ****P < .0001; ns not statistically significant.).

experiments. The results demonstrated that while the expression of cartilage-associated genes did not significantly increase under our conditions, a consistently elevated tendency was noted in the hACECM group. Our in vivo study showed that the quality of regenerated tissue treated with an hACECM-based strategy was superior to that following MF treatment in terms of both macroscopic and histological criteria.

For in vivo evaluation, we used sheep as a large animal model to mimic a full-thickness articular cartilage defect in the weight-bearing area of their hind limb femoral condyles. The results from the control group in this study, after a 12-month period, verified that critical range cartilage defects failed to regenerate a structure and composition akin to the original tissue. The defect area showed fibrous tissue filling, uneven surface ruptures, subchondral bone outgrowth towards the articular surface, local collapse, and cystic degeneration. The genesis of new tissue in defects of this size range was primarily dictated by experimental interventions, underlining the reliability and validity of our findings.

Our experiment further corroborates these findings. Broadly speaking, at the 6-month time point, the defect area in the MF group was largely filled with new tissue, yet this tissue substantially differed from the surrounding normal cartilage, demonstrating more fibrous structures, less polished surfaces, and disorganized arrangements. Histological staining underscored these results, showing localized subarticular osteophyte aggregation and inconsistent staining of the cartilage matrix

on the new tissue. These observations suggest that the new tissue in the defect area is fibrocartilage with a thin cartilage layer. The 12-month results echoed the earlier findings. Despite a gross appearance closer to normal cartilage after a longer repair period, the surface remained slightly rougher, the defect area border less integrated, and the cartilage matrix staining on the new tissue was lighter and less uniform. This suggests that the new fibrocartilage tissue in the MF group still diverged from the articular hyaline cartilage. Given its lower resistance to shear, friction, and impact, fibrocartilage yields unsatisfactory results in long-term clinical outcome observations.

At the short-term 3-month time point, cartilage defects remained significantly apparent in both experimental groups. Although the International Cartilage Repair Society (ICRS) gross perception scores differed between the experimental groups, the variation was not statistically significant. This might be attributed to the poor self-healing capacity and lack of blood nutrient supply inherent to the cartilage region. Even with local intervention, complete filling of the defect could not be achieved promptly due to weight-bearing effects and local inflammatory stimulation. Notably, the Control group presented issues including, but not limited to, substantial defect enlargement, subchondral bone exposure, and local fibrosis. Histological staining results suggested a disrupted continuity of the cartilage surface in the repaired area for each group, with the repaired areas mostly filled with fibrous tissue. A clear

demarcation between the normal tissue was observed, alongside disrupted subchondral bone morphology, with changes such as subchondral bone sclerosis and bone cyst formation prevalent in the Control and MF groups. Nevertheless, no statistical difference was observed between groups in the histological score at the 3-month mark.

As the repair time extended to 6 months, the new tissue in the experimental group filled in more comprehensively compared to the control group. The border with surrounding normal cartilage essentially vanished, indicating superior compatibility between the new tissue and the adjacent area. The new cartilage appeared visually non-fibrotic and largely resembled the normal tissue, suggesting successful cartilage regeneration in the defect area using the scaffold. The rough surface of the new tissue in the defect area might be attributable to the tissue's need to adapt to bearing pressure and friction during the regeneration process. Histological staining at this time point showed that the hACECM and hACECM/MF groups were morphologically closer to normal cartilage than the MF group, with distinct tissue layers and mature oval chondrocytes in the cartilage layer. However, the arrangement was slightly disorganized, differing from the normal longitudinal arrangement of chondrocytes. The histological score at the 6-month mark also suggested superior performance of the hACECM and hACECM/MF groups compared to the MF and the Control groups.

At the 12-month mark, both the hACECM and hACECM/MF groups exhibited better tissue filling and contouring in the gross view compared to the control group. The tissue color in most defect areas was not significantly different from that of normal cartilage, suggesting successful scaffold implantation and local platform provision for cells, leading to the formation of new tissues that closely fit the natural joint surface. Despite there being no statistical difference between the three groups in the gross body view score, the mean score of the MF group was lower than that of the hACECM and hACECM/MF groups. Histological staining observations at the 12-month time point showed significant differences: while the MF group formed cartilage-like tissue above the subchondral bone plate, the matrix staining was faint, and the cells within were mostly spindle-shaped and irregularly arranged. This suggested that the tissue was not hyaline cartilage and significantly differed from normal cartilage in terms of compression resistance. In contrast, in the hACECM and hACECM/MF groups, the cartilage matrix staining was apparent, the staining uniform, and the cells more closely resembled chondrocytes. Sirius red staining results suggested that the repair tissue in the hACECM and hACECM/MF groups contained more type II collagen tissue, and the collagen fibers were arranged longitudinally, indicating the gradual formation of normal cartilage with certain compression resistance. This result showed that although the hACECM and hACECM/MF groups did not differ significantly from the MF group in the gross view, their internal composition and structure were better than those of the MF group in the more microscopic histology.

MRI results also depicted a disruption of cartilage signal in the MF group at the 6- and 12-month stages, with the defect area filled with bone signal. This suggests the hydrogen ion content of the new tissue differed from that of the normal tissue, likely due to differences in tissue water content, a hypothesis requiring further investigation. These findings demonstrate that without cartilage protection and effective intervention, subchondral bone can suffer bone loss. The Control group displayed higher Sp compared to the other groups, indicating increased and sparse trabecular distance, leading to bone cyst formation and deep subchondral lesions.

Micro-CT scans at the 3-month mark showed significant bone collapse and subchondral bone resorption in the defect areas for all groups, indicating that the lack of cartilage protection led to a collapse of the intact subchondral bone plate in a short period, likely due to mechanical and local inflammatory stimulation. The scans also revealed that the subchondral bone in the MF group was overgrown and protruded beyond the normal subchondral bone plate plane towards the joint surface at the 6- and 12-month marks. This phenomenon could be due to the removal of the cartilage on the articular surface in the cartilage defect model,

allowing the subchondral bone to provide a growth microenvironment for the undifferentiated pluripotent stem cells entering the defect area. Consequently, the pluripotent stem cells leaned towards osteogenesis, resulting in fibrocartilage filled defects, characterized by higher type I collagen, rather than the required type II collagen production. We noted that the mean BMD, BT/TV, and Tb.Th values were higher in the MF and hACECM/MF groups compared to the hACECM group, which preserved the intact subchondral bone without drilling. The microfracture procedure necessitates drilling to a certain depth and incites local bleeding, thereby altering the subchondral bone's structure and the microenvironment of the underlying cancellous bone and bone marrow cavity. Consequently, this technique impacts the calcification and reconstruction of the cartilage-deprived subchondral bone. On the other hand, the hACECM group demonstrated morphologically stable subchondral bone repair, as seen in Micro-CT scans at each time point, with a gradual filling of the defect area. There were no significant instances of hyperplasia, excessive calcification, or bone cyst formation. This suggests that this repair methodology had the least impact on the subchondral bone compared to the other groups.

In summary, these results underscore that the hACECM scaffold provided a site conducive for cell proliferation, migration, and differentiation, leading to the regeneration of well-structured hyaline cartilage tissue in the area of articular cartilage defects. The crucial difference between the two experimental groups lies in the fact that the hACECM group preserved the intact subchondral bone, thereby causing the least disruption to the defect area's subchondral bone, maintaining stable bone structure. In contrast, the hACECM/MF group generated more hyaline cartilage tissue and superior cartilage morphology than the hACECM group due to the involvement of more pluripotent stem cells, albeit at the cost of structural alterations to the repair area's subchondral bone.

Future research must focus on the repair mechanism of this scaffold to devise better implantation methods that fulfill the repair objectives while minimally impacting the in situ tissue. Most tissue engineering techniques currently used in clinical practice require autologous cell culture followed by a second-stage combined scaffold implantation. This process not only increases the time and economic cost but also elevates the risk of infection due to multiple operations. In contrast, in this experiment, the scaffold implantation could be completed in a single operation with promising results. Moreover, the scaffold material used in this experiment, originating from human cartilage, is more conducive to tissue regeneration and elicits fewer inflammatory and immune responses in vivo than allogeneic or synthetic materials. This feature holds significant clinical application potential. However, translating the findings in this study to human patients is also faced with challenges. Firstly, the sheep knee joint cartilage thickness and biomechanical properties are different from human, and the postsurgery joint fixation and subsequently rehabilitation plan is relatively impractical which is also a critical factor may influent the cartilage repair outcomes. Besides, the healthy hACECM is relatively difficult to access and the application of this human tissue-derived ECM expect to face difficulties in ethics, large-scale, standardized preparation and preservation. Finally, a lot of cartilage injury patients are already present with OA symptom and the entire knee joint are not suitable for scaffold implantation. Therefore, these findings present in this study add to the cartilage repair knowledge may provide valuable information for researchers who consider using the hACECM for further pre-clinical animal testing of new cartilage tissue engineering applications.

It is worth mentioning that there are still several limitations in our study. Firstly, the lack of available data on the detailed biochemical contents of the repaired tissues preventing the further understating of repaired tissue. In the following study, we will use other method such as proteomic analysis to investigate the certain content and relative mechanism. Secondly, another major limitation of this study is that there were only 6 animals in each group. The power of statistical analysis was relatively low. However, the animal number should be as little as possible to fulfill the ethical principle of Reduction. In the process of experimental

design, we had consulted statisticians and referenced previous similar studies. Finally, one limitation of this study was that the longest observation period was only 12 months, preventing gain more insights into the long-term regenerative performance of the new tissues and whether better repair or progressive degeneration leading to arthritis occurs.

5. Conclusion

This study has demonstrated that hACECM scaffold combining with/without MF technique both have potential to repair full-thickness chondral defects. We fabricated hACECM scaffold successfully by a simple, effective, and low-cost method. Furthermore, we validated the capacity of the hACECM scaffold to support the survival, proliferation, migration, and maintenance of the human chondrocyte phenotype in vitro. Our in vivo experimentation showcased the scaffold's ability to repair articular cartilage in large animals independently. Given its safety and effectiveness, the hACECM scaffold holds promise for broad application in cartilage tissue engineering in the future. To gain a deeper understanding of the underlying mechanisms of chondral repair, further research is necessary.

Author contributions

Shuyun Liu, Quanyi Guo: Conceptualization, Methodology, Software, Liqing Peng, Hao Li, Haoyuan Deng: Data curation, Writing-Original draft preparation, Tianze Gao, Runmeng Li: Visualization, Ziheng Xu, Qinyu Tian: Investigation, Shuyun Liu, Quanyi Guo: Supervision, Tianyuan Zhao, Jianwei Li, Yongkang Yang, Chao Wang: Software, Validation, Liqing Peng, Hao Li: Writing- Reviewing and Editing, All the authors above approved the version of the manuscript to be published.

Declaration of competing interest

All authors involved in this article declare that there are no conflicts of interest regarding the publication of this paper.

Acknowledgements

References

[1] Yan W, Xu X, Xu Q, Sun Z, Lv Z, Wu R, et al. An injectable hydrogel scaffold with kartogenin-encapsulated nanoparticles for porcine cartilage regeneration: a 12-month follow-up study. Am J Sports Med 2020;48(13):3233–44.
[2] Cortese F, McNicholas M, Janes G, Gillogly S, Abelow SP, Gigante A, et al. Arthroscopic delivery of matrix-induced autologous chondrocyte implant: international experience and technique recommendations. Cartilage 2012;3(2):156–64.
[3] Thorup A-S, Strachan D, Caxaria S, Poulet B, Thomas BL, Eldridge SE, et al. ROR2 blockade as a therapy for osteoarthritis. Sci Transl Med 2020;12(561):eaax3063.
[4] Negoro T, Takagaki Y, Okura H, Matsuyama A. Trends in clinical trials for articular cartilage repair by cell therapy. NPJ Regenerative medicine 2018;3(1):17.
[5] Roseti L, Grigolo B. Current concepts and perspectives for articular cartilage regeneration. J Experimental Orthopaedics 2022;9(1):61.
[6] Musumeci G, Aiello FC, Szychlinska MA, Di Rosa M, Castrogiovanni P, Mobasheri A. Osteoarthritis in the XXIst century: risk factors and behaviours that influence disease onset and progression. Int J Mol Sci 2015;16(3):6093–112.
[7] Mithoefer K, McAdams T, Williams RJ, Kreuz PC, Mandelbaum BR. Clinical efficacy of the microfracture technique for articular cartilage repair in the knee: an evidence-based systematic analysis. Am J Sports Med 2009;37(10):2053–63.
[8] Aae TF, Randsborg P-H, Lurås H, Årøen A, Lian ØB. Microfracture is more cost-effective than autologous chondrocyte implantation: a review of level 1 and level 2 studies with 5 year follow-up. Knee Surg Sports Traumatol Arthrosc 2018;26:1044–52.
[9] Kraeutler MJ, Belk JW, Purcell JM, McCarty EC. Microfracture versus autologous chondrocyte implantation for articular cartilage lesions in the knee: a systematic review of 5-year outcomes. Am J Sports Med 2018;46(4):995–9.
[10] Martín AR, Patel JM, Zlotnick HM, Carey JL, Mauck RL. Emerging therapies for cartilage regeneration in currently excluded 'red knee'populations. NPJ Regenerative medicine 2019;4(1):12.
[11] Atala A, Kasper FK, Mikos AG. Engineering complex tissues. Sci Transl Med 2012;4(160). 160rv12-160rv12.
[12] Xing H, Lee H, Luo L, Kyriakides TR. Extracellular matrix-derived biomaterials in engineering cell function. Biotechnol Adv 2020;42:107421.
[13] Tamaddon M, Burrows M, Ferreira S, Dazzi F, Apperley J, Bradshaw A, et al. Monomeric, porous type II collagen scaffolds promote chondrogenic differentiation of human bone marrow mesenchymal stem cells in vitro. Sci Rep 2017;7(1):43519.
[14] Mahon OR, Browe DC, Diaz-Payno PJ, Pitacco P, Cunningham KT, Mills KH, et al. Extracellular matrix scaffolds derived from different musculoskeletal tissues drive distinct macrophage phenotypes and direct tissue-specific cellular differentiation. J Immunol Regenerative Medicine 2021;12:100041.
[15] Yoon DS, Lee K-M, Kim S-H, Kim SH, Jung Y, Kim SH, et al. Synergistic action of IL-8 and bone marrow concentrate on cartilage regeneration through upregulation of chondrogenic transcription factors. Tissue Eng 2016;22(3–4):363–74.
[16] Kim JH, Lee MC, Seong SC, Park KH, Lee S. Enhanced proliferation and chondrogenic differentiation of human synovium-derived stem cells expanded with basic fibroblast growth factor. Tissue Eng 2011;17(7–8):991–1002.
[17] Liu Y, Ma N, Zhao Z, Guo Q. Mid-to long-term clinical outcomes of cartilage restoration of knee joint with allogenic next-generation matrix-induced autologous chondrocyte implantation (MACI). Orthop Surg 2023;15(2):549–62.
[18] Yang Z, Cao F, Li H, He S, Zhao T, Deng H, et al. Microenvironmentally optimized 3D-printed TGFβ-functionalized scaffolds facilitate endogenous cartilage regeneration in sheep. Acta Biomater 2022;150:181–98.
[19] Tian G, Jiang S, Li J, Wei F, Li X, Ding Y, et al. Cell-free decellularized cartilage extracellular matrix scaffolds combined with interleukin 4 promote osteochondral repair through immunomodulatory macrophages: in vitro and in vivo preclinical study. Acta Biomater 2021;127:131–45.
[20] Zheng X-F, Lu S-B, Zhang W-G, Liu S-Y, Huang J-X, Guo Q-Y. Mesenchymal stem cells on a decellularized cartilage matrix for cartilage tissue engineering. Biotechnol Bioproc Eng 2011;16(3).
[21] Zhang Y, Hao C, Guo W, Peng X, Wang M, Yang Z, et al. Co-culture of hWJMSCs and pACs in double biomimetic ACECM oriented scaffold enhances mechanical properties and accelerates articular cartilage regeneration in a caprine model. Stem Cell Res Ther 2020;11(1):1–13.
[22] Munirah S, Samsudin O, Chen H, Salmah SS, Aminuddin B, Ruszymah B. Articular cartilage restoration in load-bearing osteochondral defects by implantation of autologous chondrocyte-fibrin constructs: an experimental study in sheep. The Journal of Bone & Joint Surgery British 2007;89(8):1099–109.
[23] Martinez-Carranza N, Berg H, Hultenby K, Nurmi-Sandh H, Ryd L, Lagerstedt A-S. Focal knee resurfacing and effects of surgical precision on opposing cartilage. A pilot study on 12 sheep, Osteoarthritis and Cartilage 2013;21(5):739–45.
[24] Martinez-Carranza N, Ryd L, Hultenby K, Hedlund H, Nurmi-Sandh H, Lagerstedt A, et al. Treatment of full thickness focal cartilage lesions with a metallic resurfacing implant in a sheep animal model, 1 year evaluation. Osteoarthritis Cartilage 2016;24(3):484–93.
[25] Brittberg M, Peterson L. Introduction of an articular cartilage classification. ICRS newsletter 1998;1(1):5–8.
[26] Peterfy C, Guermazi A, Zaim S, Tirman P, Miaux Y, White D, et al. Whole-organ magnetic resonance imaging score (WORMS) of the knee in osteoarthritis. Osteoarthritis Cartilage 2004;12(3):177–90.
[27] Goebel L, Orth P, Müller A, Zurakowski D, Bücker A, Cucchiarini M, et al. Experimental scoring systems for macroscopic articular cartilage repair correlate with the MOCART score assessed by a high-field MRI at 9.4 T–comparative evaluation of five macroscopic scoring systems in a large animal cartilage defect model. Osteoarthritis Cartilage 2012;20(9):1046–55.
[28] Cunniffe GM, Díaz-Payno PJ, Sheehy EJ, Critchley SE, Almeida HV, Pitacco P, et al. Tissue-specific extracellular matrix scaffolds for the regeneration of spatially complex musculoskeletal tissues. Biomaterials 2019;188:63–73.
[29] Williams 3rd RJ, Harnly HW. Microfracture: indications, technique, and results. Instr Course Lect 2007;56:419–28.
[30] Sommerfeldt MF, Magnussen RA, Hewett TE, Kaeding CC, Flanigan DC. Microfracture of articular cartilage. JBJS reviews 2016;4(6):e6.
[31] Zhang Y, He Y, Bharadwaj S, Hammam N, Carnagey K, Myers R, et al. Tissue-specific extracellular matrix coatings for the promotion of cell proliferation and maintenance of cell phenotype. Biomaterials 2009;30(23–24):4021–8.
[32] Badylak SF. The extracellular matrix as a biologic scaffold material. Biomaterials 2007;28(25):3587–93.
[33] Browe DC, Burdis R, Díaz-Payno PJ, Freeman FE, Nulty JM, Buckley CT, et al. Promoting endogenous articular cartilage regeneration using extracellular matrix scaffolds. Materials Today Bio 2022;16:100343.
[34] Díaz-Payno PJ, Browe DC, Cunniffe GM, Kelly DJ. The identification of articular cartilage and growth plate extracellular matrix-specific proteins supportive of either osteogenesis or stable chondrogenesis of stem cells. Biochem Biophys Res Commun 2020;528(2):285–91.